Anti-Cancer Drugs 1994, **5**, pp. 160–170

Computer-assisted microscope analysis of morphonuclear modifications induced by anticancer antimetabolites in cell lines cultured *in vitro*

Olivier Pauwels,[1,2] Robert Kiss[2] and Ghanem Atassi[1,3]

[1]Laboratory of Cell Pharmacology, Institute of Pharmacy, Free University of Brussels, Boulevard du Triomphe, 1050 Brussels, Belgium. [2]Laboratory of Histology, Faculty of Medicine, Free University of Brussels, 808 route de Lennik, 1070 Brussels, Belgium. Tel: (+32) 2 555 63 80; Fax: (+32) 2 555 62 85. [3]Institut de Recherches Servier, 14 rue de la République, 92150 Suresnes, France.

An original method is proposed for the purpose of discriminating between antimetabolites exhibiting different operating mechanisms. The present work was carried out by means of the digital cell image analysis of Feulgen-stained nuclei cultured in the presence of different antimetabolites. We chose this method because it enables anticancer drug-induced effects to be studied at both morphonuclear and cell cycle levels in the same biological sample. The results show that all the antimetabolites had similar effects on the nuclear texture of the cells and on cell cycle parameters. Furthermore, the use of multivariate analyses made it possible to distinguish between different mechanisms of action among drugs belonging to the same class of antineoplastic, i.e. antimetabolite agents.

Key words: Antimetabolites, cell kinetic, image analysis, multivariate analysis.

Introduction

A large number of methods exist for the study of operating mechanisms of antineoplastic drugs. Often, it is the operating mechanism which dictates the method used. For example, antineoplastic drugs, which act through an interaction with the DNA (e.g. alkylating and intercalating agents), are studied by means of an alkaline elution technique.[1,2] The operating mechanism of vinca alkaloids, which includes alterations to the spindle microtubule dynamics, can be studied by means of specific biochemical methods.[3,4] The operating mechanism of antimetabolites is often monitored by means of radiolabeled molecules.[5,6]

OP is the holder of a grant from the 'Fonds National de la Recherche Scientifique' (FNRS, Belgium). RK is a Research Associate with the FNRS, Belgium.

Correspondence to R Kiss

We reported previously that it is possible to study the effects of several kinds of antineoplastic drugs by means of digital cell image analysis.[7] In this earlier work we demonstrated that image analysis makes it possible to study the effects of anticancerous drugs on several levels of biological cell characteristics, i.e. proliferation, the distribution of the cells in the cell cycle and chromatin pattern characteristics. Furthermore, the combined use of multivariate analyses (principal components analysis with the canonical transformation of the data followed by discriminant linear analyses of the digital image analysis of Feulgen-stained nuclei) enabled us to distinguish between several classes of antineoplastic drugs (e.g. alkylating agents and anthracyclines) on the basis of the quantitative description of the chromatin pattern.[7]

In the present work, we report the specific effects caused by several antimetabolites at the three biological cell characteristic levels mentioned above, i.e. proliferation, cell cycle kinetics and chromatin pattern characteristics. These effects were carried out by means of the digital cell image analyses of Feulgen stained-nuclei[8] from three distinct neoplastic cell lines cultured *in vitro*, i.e. the MTX mouse mammary cell line,[9] and the J82[10] and T24[11] vesical cell lines, each of which was treated with five different antimetabolite agents. The five agents under study were from three distinct classes of antimetabolite drugs as classified by Black and Livingston.[12] The five compounds involved the folic acid antagonists, which included methotrexate (MTX); the pyrimidine analogs, which included 5-fluorouracil (5-FU) and cytarabine (ARA-C); and the purine analogs, which included 6-mercaptopurine (MP) and 6-thioguanine (TG). Pentostatin, which is classified as an adenosine deaminase inhibitor, was not studied here.

Using multivariate analyses of the data relating to the drug-induced effects at morphonuclear, i.e. chromatin pattern, level, we also tried in our current work to distinguish between the several operating mechanisms of the five antimetabolite agents under study.

Materials and methods

Drugs

MTX, 5-FU and ARA-C came from Sigma (St Louis, MO). MP and TG came from Wellcome (Aalst-Erembodegem, Belgium).

Cell culture

The MTX cell line was established to grow *in vitro*[9] from the MTX mouse mammary adenocarcinoma.[13] The other cell lines were from the American Type Culture Collection. These were the J82 (HTB 1) and T24 (HTB 4) cell lines, which originated in two human bladder cancers. These three cell lines were cultured as previously described.[7] Briefly, the cells were cultured at a temperature of 37°C in an atmosphere containing 5% CO_2. The culture medium consisted of Eagle's minimum essential medium (MEM) supplemented with 5% fetal calf serum, L-glutamine and antibiotics (all the solutions were from Gibco, Paisley, UK).

Preparation of the samples

The preparation of the samples has been described elsewhere.[7] Briefly, aliquots of 2.5 ml of a suspension containing 25 000 cells in the exponential growth phase were plated in Petri dishes with a diameter of 35 mm (Nunc, Roskilde, Denmark). Each Petri dish contained a glass microscope slide to which the cells were able to adhere. After 24 h of incubation, the medium was supplemented with the different antimetabolite agents in various concentrations in order to obtain different final concentrations of these agents, i.e. 10^{-7}, 10^{-8}, 10^{-9}, 10^{-10} and 10^{-11} M for MTX; 10^{-4}, 10^{-5}, 10^{-6}, 10^{-7} and 10^{-8} M for 5-FU; 10^{-4}, 10^{-5}, 10^{-6}, 10^{-7} and 10^{-8} M for ARA-C; 10^{-3}, 10^{-4}, 10^{-5}, 10^{-6} and 10^{-7} M for MT; 10^{-4}, 10^{-5}, 10^{-6}, 10^{-7} and 10^{-8} M for TG. The control condition (CT) included cell lines cultured in the absence of any drugs. Seventy-two hours after the addition of the drugs, the slides were fixed in a mixture of ethanol 96% (75 ml), formol 40% (20 ml) and acetic acid 100% (5 ml) (EFA), and mounted on microscope slides by means of DPX (BDH Chemicals, Poole, UK). The slides were stained by means of the Feulgen reagent (Fluka, Buchs, Switzerland) after hydrolysis in 6N HCl for 1 h at 24°C.[8] These slides were used to study antimetabolite agents induced effects on both the cell growth and the morphonuclear features of the cell lines.

Cell growth assessment

The number of cells present on an area of 16 mm^2 was counted for each slide analyzed. This was carried out using a microscope equipped with a 100-square grid. Five areas were analyzed per slide and, thus, 15 areas per experimental conditions. The values so obtained enabled the cytotoxic effect of the antimetabolites on the proliferation of the cell lines to be recorded.

Image analysis

For each experimental condition 900 nuclei were analyzed by means of a SAMBA 2005 system (Alcatel-TITN, Grenoble, France). These nuclei came from a merged file containing the digitized images of the 300 cell nuclei from each triplicate. Each nucleus was characterized by means of 15 morphonuclear parameters[14] belonging to four groups. The first group included one geometric parameter, i.e. the nuclear area (NA, parameter 1), which describes nuclear size. The second group included five densitometric parameters. These were integrated optical density (IOD, parameter 2), which measures the nuclear DNA content[15]; the mean optical density (MOD, parameter 3); the variance of optical density (VOD, parameter 5); and the skewness (SK, parameter 4) and kurtosis (K, parameter 6) indices. Of these five parameters, only the IOD is really a densitometric parameter because the other four in fact describe the chromatin texture from a densitometric point of view. The final two groups of parameters also quantitatively describe the chromatin texture pattern. The third group includes five parameters which were computed on the basis of the length section matrices.[16] These were the frequency of short (SRL, parameter 7) and long (LRL, parameter 8) run length emphases, which are representative of the frequency of small and large dense chromatin clumps, respectively; their distributions (RLD, parameter 10); their percentage (RLP, parameter

11); and the gray level distribution (GLD, parameter 9). The fourth group included four parameters computed on the basis of the co-occurrence matrices.[17] It included the local mean (LM, parameter 12), energy (E, parameter 13), the coefficient of variance (CV, parameter 14), which measure the level of overall chromatin condensation; and contrast (C, parameter 15), which is representative of the number of boundaries between nuclear regions with distinct optical densities.

Statistical and mathematical analyses

The assessments of cell growth and morphonuclear characteristics are reported as means (± SEM) statistically compared by means of the Fisher *F*-test (one-way variance analysis). The equality of variance was checked by the Bartlett test. The levels of statistical significance reported in the figures are: $*p < 0.05$; $**p < 0.01$; $***p < 0.001$.

We also used principal component analysis followed by the canonical transformation of the data in order to characterize 'typical' cell nuclei from the different nuclei populations submitted to different antimetabolites agents. These analyses involved the multivariate analysis described by Bartels.[18] The assessment of the proportion of cells in the various phases of the cell cycle was carried out by means of linear discriminant analysis with reference to specific 'morphonuclear data banks' related to the G_0–G_1, S, G_2 and M phases of the cell cycle. These four data banks were also obtained by means of principal component analysis followed by the canonical transformation of the data by means of a methodology described previously.[7,19,20]

Results

Cell growth

Figure 1 illustrates the cell growth in those experimental conditions where a significant drug-induced effect (with at least $p < 0.05$) was observed in cell growth but where a significant proportion of the cell nuclei were still present, so making digital cell image analysis possible.

The results show that of the five antimetabolites used, the MTX was the most effective. Indeed, at a concentration of 10^{-7} M, this drug killed 90 and 77% of the MTX and J82 cells, respectively, while the other antimetabolites induced a maximum decreased between 78% (5-FU in the MTX cell line)

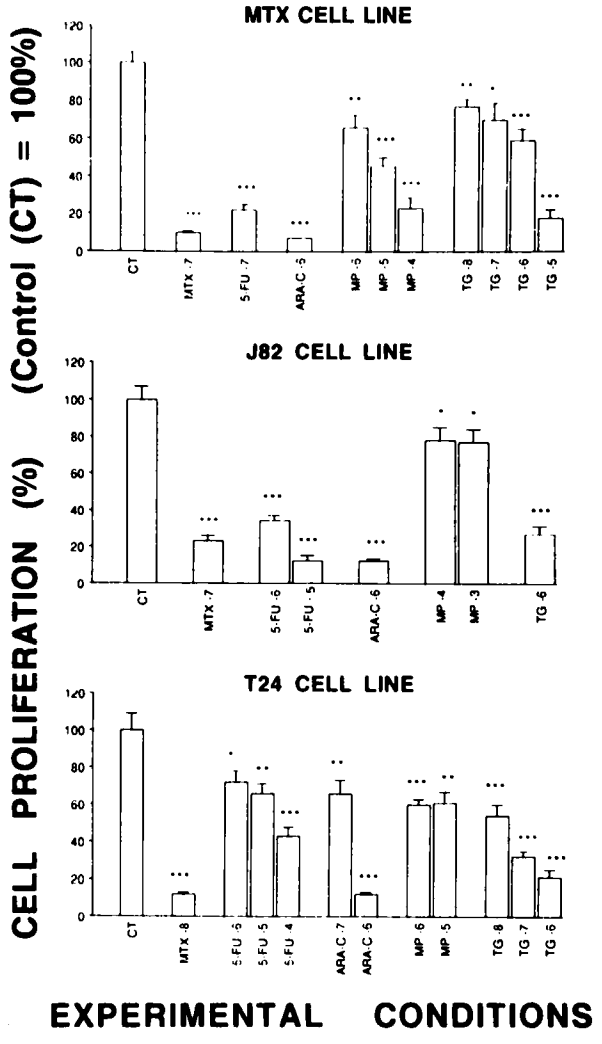

Figure 1. The cell proliferation levels recorded in the MTX mouse mammary and the J82 and T24 human bladder cancer cell lines after the incubation of these cells in several concentrations of five distinct antimetabolite agents (the concentrations are given as logarithms). The five antimetabolite agents involve a folic acid antagonist (MTX), two pyrimidine analogs (5-FU and ARA-C) and two purine analogs (MP and TG). The results are expressed in mean percentage values of the proliferation level compared to the control value (CT ± SEM) ($*p < 0.05$; $**p < 0.01$; $***p < 0.001$).

and 29% (ARA-C in the J82 cell line) in cell proliferation (Figure 1). On the other hand, a 10^{-8} M concentration of MTX induced the death of 88% of the T24 cells while the remaining four antimetabolites did not have any significant effects ($p > 0.05$) on this cell line (data not shown) at this concentration, except in the case of the TG, which killed 46% of the cells. With respect to the pyrimidine (5-FU and ARA-C) and purine (MP and TG) analogs, Figure 1 shows that the pyrimidine analogs were usually

more active against the three cell lines tested than the purine analogs. For example, a concentration of 10^{-6} M of 5-FU and ARA-C caused the death of 90 and 93% of the MTX cells, respectively, while at this concentration MP and TG killed 34 and 41% of the MTX cell only. We nevertheless observed two exceptions concerning the J82 and T24 cell lines. In the case of the J82 line, the effects of the 5-FU and TG were not significantly different ($p > 0.05$) when the same concentrations, i.e. 10^{-6} M, were considered. In the case of the T24 line, results show that MP acted with the same efficiency as the 5-FU at the concentration of 10^{-6} and 10^{-5} M, and that the TG was more effective than the 5-FU against the T24 cells for all the concentrations under study ($p < 0.05$ to $p < 0.001$).

Image analysis

Monovariate analyses. Figure 2 illustrates the effects of the five antimetabolites on the mean nuclear area value (NA). The mean NA value significantly increased ($p < 0.001$ or $p < 0.01$ in the case of the T24 cell line treated with 10^{-5} M MP). One exception was observed; thus, the 5-FU produced either no significant effects ($p > 0.05$) on the T24 cells or only a slight but nevertheless statistically significant decrease ($p < 0.05$) in this mean parameter value at the concentrations of 10^{-6} and 10^{-5} M, respectively. At the concentrations of 10^{-4} M, the general' rule was confirmed, i.e. the mean NA value increased ($p < 0.001$) significantly.

Similar observations were made when the mean integrated optical density (IOD) value was considered (Figure 3). Indeed, this parameter usually increased under antimetabolite agent treatment. Nevertheless, in some cases, we observed no statistical effects with respect to the action of the drugs on this mean parameter value ($p > 0.05$). In the case of the T24 cell line treated with 10^{-6} M 5-FU, a slight but significant decrease ($p < 0.01$) in the mean IOD was even observed. These drug-induced effects recorded for the nuclear DNA content—as globally assessed by means of the IOD parameter—were studied further by assessing the proportion of control and drug-treated cells in the G_0–G_1, S, G_2 and M phases of the cell cycle. This is illustrated in Tables 1 (MTX cell line), 2 (J82 cell line) and 3 (T24 cell line). The results given in Tables 1–3 indicate that all the antimetabolites led to a decrease in the proportion of cells in the G_0–G_1 phase together with a concomitant increase in the proportion of cells present in the S and/or G_2 phases. This explains the increase

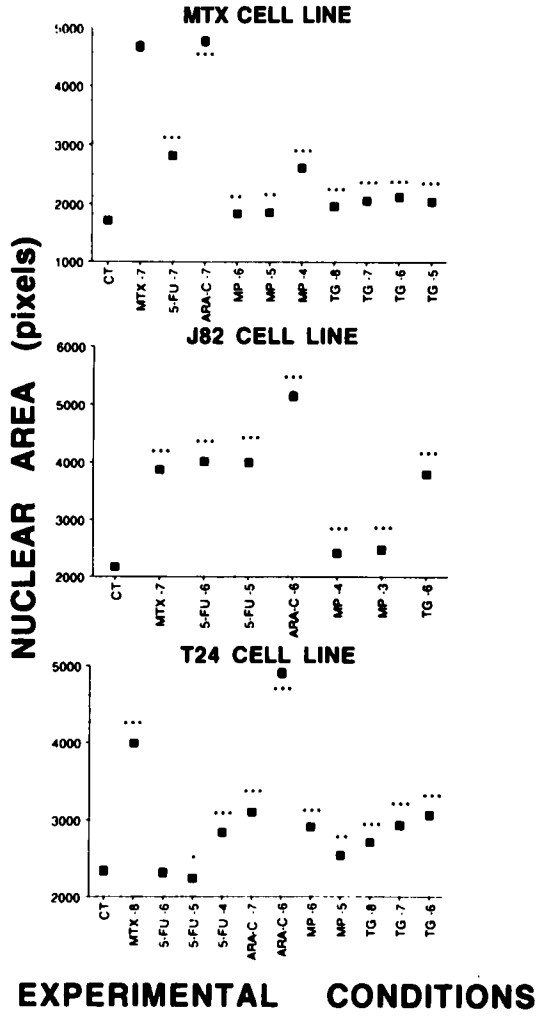

Figure 2. The development of the values of the nuclear area (NA) parameter (±SEM) under the different experimental conditions described in the legend to Figure 1. The antimetabolite concentrations are given as logarithms. The significance of the results is given in comparison with the CT condition (*$p < 0.05$; **$p < 0.01$; ***$p < 0.001$).

observed in the mean IOD values. The decrease in the mean IOD value observed in the case of the T24 cell line treated with 10^{-6} M 5-FU is explained by the fact that this drug at this concentration induced a slight decrease in the proportion of cells present in the S phase of the cell cycle.

Figure 4 describes the effects induced by the five antimetabolites in the mean long run length emphasis (LRL) value. This mean value was increased by each of the antimetabolites tested (Figure 4). This effect was significant ($p < 0.01$ or $p < 0.001$) except in the case of the T24 cell line submitted to 5-FU (10^{-6} and 10^{-5} M) or MP (10^{-5} M) ($p > 0.05$).

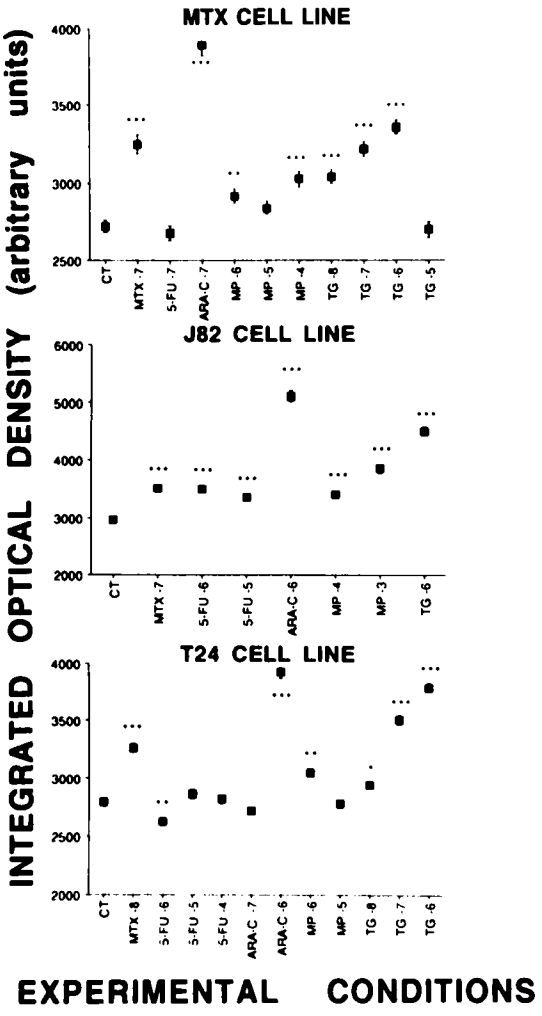

Figure 3. The development of the values of the integrated optical density (IOD) parameter (±SEM) under the different experimental conditions described in the legend to Figure 1. The antimetabolite concentrations are given as logarithms. The significance of the results is given in comparison with the CT condition (*$p < 0.05$; **$p < 0.01$; ***$p < 0.001$).

Similar observations were made when the effects of the antimetabolites on the mean local mean (LM) value were considered (Figure 5). Indeed, the antimetabolite agents induced an increase in the mean parameter value of this parameter. In the case of the MTX cells, this effect was highly significant ($p < 0.001$) except in the cases of the MP (10^{-6} and 10^{-5} M) and the TG (10^{-5} M). For the J82 cell line, the increase in the mean LM value was also highly significant ($p < 0.001$), except ($p > 0.05$) when this line had been treated with the MP. For the T24 cells, the effect was also significant ($p < 0.01$ or $p < 0.05$ in the case of MP treatment at 10^{-5} M), except ($p > 0.05$) in the cases where these cells had been

Table 1. The cycle effects of antimetabolites on the MTX cell line

	Concentration (M)	G_0–G_1	S	G_2	M
CT		61 ± 2	17 ± 0	22 ± 2	1 ± 0
MTX	10^{-7}	39 ± 6	24 ± 4	37 ± 10	0 ± 0
5-FU	10^{-7}	59 ± 5	20 ± 3	21 ± 3	0 ± 0
ARA-C	10^{-6}	25 ± 6**	24 ± 1**	51 ± 4**	0 ± 0
MP	10^{-6}	53 ± 4	23 ± 0	24 ± 4	0 ± 0
	10^{-5}	53 ± 7	21 ± 1	26 ± 5	0 ± 0
	10^{-4}	46 ± 3**	24 ± 2	30 ± 3	0 ± 0
TG	10^{-8}	49 ± 3	22 ± 3	32 ± 3	0 ± 0
	10^{-7}	43 ± 3	18 ± 1	38 ± 3**	0 ± 0
	10^{-6}	35 ± 5**	13 ± 1	52 ± 5**	0 ± 0
	10^{-5}	62 ± 5	15 ± 2	23 ± 7	0 ± 0

The effects of the antimetabolites on the distribution of the MTX cells in the cell cycle for each concentration studied. The results are given in percentage ± SEM. The significance of the results is given in comparison with the CT condition (*$p < 0.05$; **$p < 0.01$; ***$p < 0.001$).

treated with 5-FU at the concentrations of 10^{-6} and 10^{-5} M.

Multivariate analyses. Figures 6 and 7 report the results obtained by means of multivariate analysis relying upon the use of 15 parameters quantitatively describing morphonuclear features. The nuclear populations submitted to each of the five antimetabolites agents are reported in Figures 6 and 7. Furthermore, for each of the antimetabolites, only one concentration is illustrated in Figures 6 and 7, i.e. the one that produced the most marked effects on the 15 morphonuclear parameters. The importance of the effects are objectified by the '*a*:*b*' values depicted in Table 4. The '*a*' value represents the percentage of well-classified nuclei (WCN) assessed by means of a linear non-supervised stepwise discriminant analysis which made it possible to calculate the *F* value for each of the 15 parameters where a statistical comparison had been carried out between the CT and the drug treated cells of a given cell line for a given drug. The '*b*' value corresponds to the highest *F* value so obtained and relates to the parameter discriminating the most effectively between the CT cells and the drug-treated ones in a given cell line treated by a given drug. Thus with reference to the results presented in Table 4, Figures 6(A and B) and 7(A and B) correspond to the MTX cells treated with 10^{-7} M MTX, 10^{-7} M 5-FU, 10^{-6} M ARA-C, 10^{-4} M MP and 10^{-6} M TG; Figures 6(C and D) and 7(C and D) the J82 cells treated with 10^{-7} M MTX, 10^{-5} M 5-FU, 10^{-6} M ARA-C, 10^{-6} M MP and 10^{-7} M TG; Figures 6(E and F) and 7(E and F) the

Table 2. The cycle effects of antimetabolites on the J82 cell line

	Concentration (M)	G_0–G_1	S	G_2	M
CT		55 ± 4	24 ± 1	19 ± 4	1 ± 0
MTX	10^{-7}	25 ± 5**	39 ± 2**	36 ± 3*	0 ± 0
5-FU	10^{-6}	20 ± 2**	45 ± 1***	35 ± 2*	0 ± 0
	10^{-5}	39 ± 6	33 ± 3	28 ± 3	0 ± 0
ARA-C	10^{-6}	6 ± 1***	27 ± 1	67 ± 2***	0 ± 0
MP	10^{-4}	57 ± 3	27 ± 2	15 ± 4	0 ± 0
	10^{-3}	53 ± 5	23 ± 3	24 ± 4	1 ± 0
TG	10^{-6}	16 ± 8*	31 ± 5	52 ± 13	0 ± 0

Effects of the antimetabolites on the distribution of the J82 cells in the cell cycle for each concentration studied. The results are given in percentage ± SEM. The significance of the results is given in comparison with the CT condition (*$p < 0.05$; **$p < 0.01$; ***$p < 0.001$).

T24 cells treated with 10^{-8} M MTX, 10^{-4} M 5-FU, 10^{-6} M ARA-C, 10^{-6} M MP and 10^{-7} M TG.

Figure 6 was drawn up according to the first and second, and Figure 7 according to the first and third canonical functions. These canonical functions represent a linear combination of the 15 parameters used. This canonical treatment of data allows a projection into a two-dimensional space (the canonical space) of the 15-dimensional space corresponding to the multiparametric image featuring the 15 parameters computed on each nucleus. Figures 6(A, C and E) and 7(A, C and E) represent a comparison between the factorial cell distributions of the cell nuclei from the MTX, J82 and T24 cell lines after submission to the various antimetabolites. The ellipses represent the 95% confidence interval around the mean position of the factorial cell distribution of the different nuclear populations. Figures 6(B, D and F) and 7(B, D and F) represent the canonical projection of the 15 parameters onto the canonical plane. This projection made it possible to indicate the direction and strength of the parameter scattering for the cell populations under analysis.

Figure 6(A, C and E), which relies upon the representation of the first two canonical functions, show that these two functions made it possible to distinguish between all of the drugs tested. Figure 6(B, D and F) shows that parameters 1 (NA), 8 (LRL), 11 (RLP), 12 (LM), 13 (E), 14 (CV) and 15 (C) mostly influenced the position of the ellipses corresponding to each antimetabolite in the first canonical function. Indeed, there were parameters which exhibited the largest projection onto the first canonical function. In contrast, the position of the ellipses for the second canonical function seemed to be influenced by the nature of the cell line. Parameter 3 (MOD) thus appeared to be the strongest as compared with the second canonical function, i.e. the parameter which exhibited the largest projection onto the second canonical function. In the case of the J82 cell line, it was parameter 2 (IOD) which exhibited the largest projection onto the second canonical function, while in the case of the T24

Table 3. The cell cycle effects of antimetabolites on the T24 cell line

	Concentration (M)	G_0-G_1	S	G_2	M
CT		64 ± 1	16 ± 3	18 ± 3	3 ± 1
MTX	10^{-8}	21 ± 3***	47 ± 2***	31 ± 2	1 ± 0
5-FU	10^{-6}	64 ± 2	12 ± 1	23 ± 2	1 ± 0
	10^{-5}	59 ± 8	22 ± 2	19 ± 6	1 ± 0
	10^{-4}	35 ± 2	28 ± 3*	37 ± 3*	0 ± 0
ARA-C	10^{-7}	54 ± 4	35 ± 2**	10 ± 2	1 ± 0
	10^{-6}	17 ± 3***	26 ± 1*	57 ± 3***	0 ± 0
MP	10^{-6}	46 ± 3*	18 ± 1	35 ± 4*	1 ± 0
	10^{-5}	53 ± 3	23 ± 2	23 ± 1	1 ± 0
TG	10^{-8}	42 ± 4*	29 ± 1**	29 ± 3	0 ± 0
	10^{-7}	29 ± 1***	23 ± 2	47 ± 2***	0 ± 0
	10^{-6}	21 ± 2	22 ± 1	56 ± 2***	0 ± 0

Effects of the antimetabolites on the distribution of the T24 cells in the cell cycle for each concentration studied. The results are given in percentage ± SEM. The significance of the results is given in comparison with the CT condition (*$p < 0.05$; **$p < 0.01$; ***$p < 0.001$).

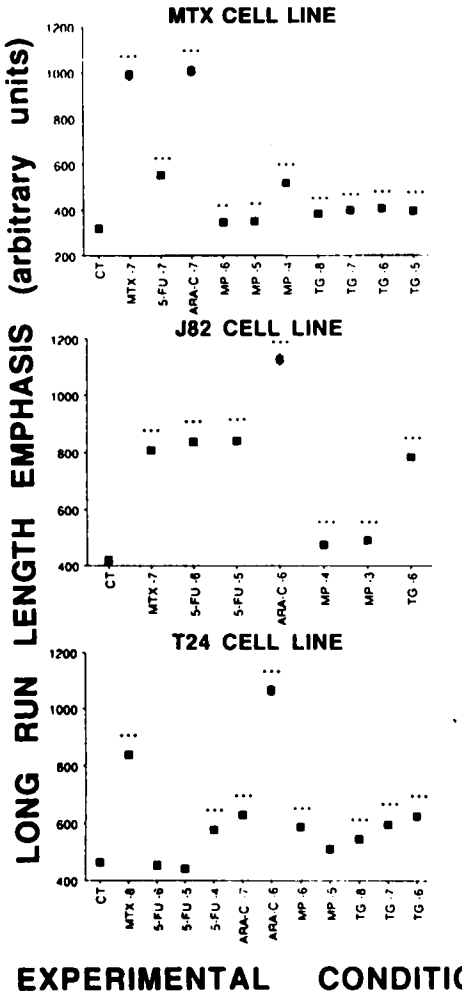

Figure 4. The development of the values of the long run length emphasis (LRL) parameter (± SEM) under the different experimental conditions described in the legend to Figure 1. The antimetabolite concentrations are given in logarithms. The significance of the results is given in comparison with the CT condition (*$p < 0.05$; **$p < 0.01$; ***$p < 0.001$).

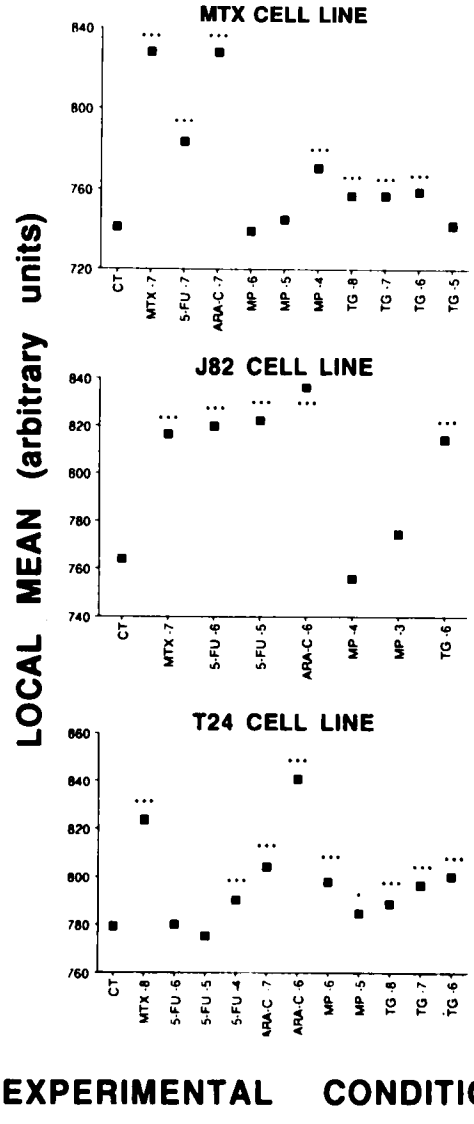

Figure 5. The values of the local mean (LM) parameter (± SEM) under the different experimental conditions described in the legend to Figure 1. The antimetabolite concentrations are given in logarithms. The significance of the results is given in comparison with the CT condition (*$p < 0.05$; **$p < 0.01$; ***$p < 0.001$).

line it was parameter 5 (VOD). In summary, the first canonical function is mainly explained in terms of the geometric parameter (NA) and of parameters computed on the basis of the length section matrices (LRL and RLP) or the co-occurrence matrices (LM, E, CV and C). In contrast, the second canonical function is mainly explained in terms of densitometric parameters (e.g. IOD, MOD, VOD).

Figure 7 illustrates the position of the ellipses describing the influence of each antimetabolite as it is explained by means of the first and the third canonical functions (Figure 7A, C and E), at the same time, Figure 7 gives the canonical projection of the 15 parameters onto the canonical plane (Figure 7B, D and F). The third canonical function is mainly explained by means of the K, SK, LM and E parameters in the case of the MTX cell line (Figure 7B), by the LRL parameter in the case of the J82 line (Figure 7D) and by the IOD parameter in the case of T24 line (Figure 7E). It appears that the position of the ellipses made it possible to discriminate not only between each drug under study, but also between the different pharmacological classes of the antimetabolite agents under study. Indeed, it was possible to divide the canonical plane into three areas

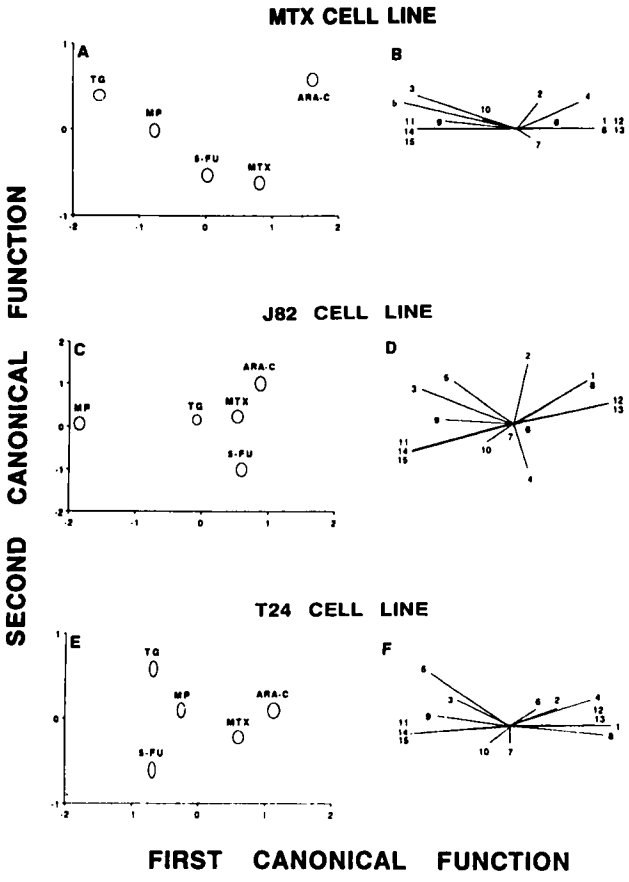

Figure 6. The results obtained after performing multivariate analyses on the drug-induced morphonuclear modification recorded on 900 nuclei from merged files containing the digitized nuclear images relating to MTX-, 5-FU-, ARA-C-, MP- and TG-treated MTX (A and B), J82 (C and D) and T24 (E and F) cell lines). Each nucleus was described by means of 15 morphonuclear parameters and submitted to principal components analysis. The nuclei were thus located in a 15-dimensional space on the basis of their 15 nuclear parameters. They were then projected into a two-dimensional space by the canonical transformation of their data. This two-dimensional space is defined by the first two canonical functions. Charts A, C and E represent complex multifactorial functions featuring the nuclei. Each ellipsis represents the 95% confidence interval around the mean position of the factorial cell distribution. Charts B, D and F represent the canonical projection of the 15 parameters. This projection indicates the direction and strength of the parameter scattering for the cell populations under analysis. See text for the significance of each parameter.

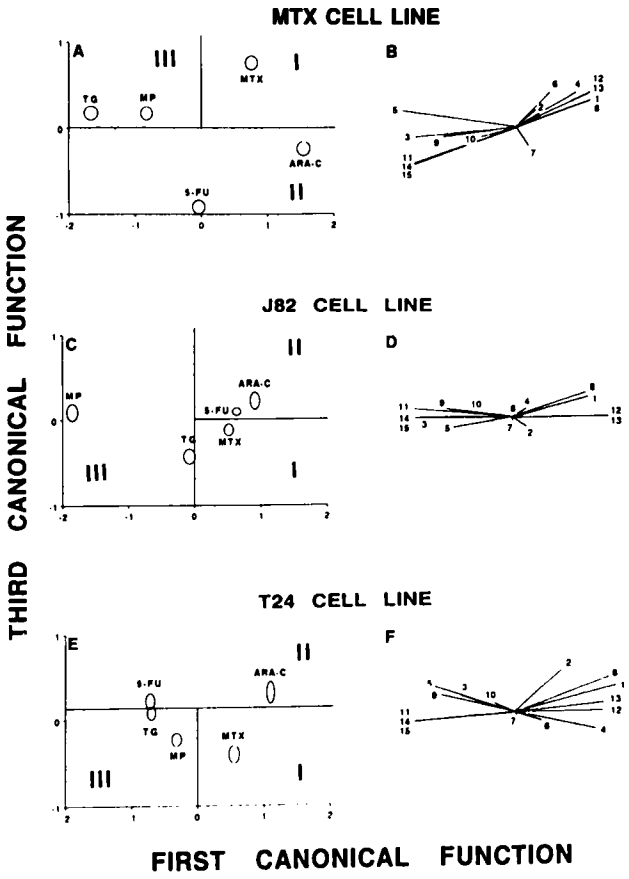

Figure 7. The results obtained after performing the same multivariate analysis as described in Figure 6, i.e. relating to MTX-, 5-FU-, ARA-C-, MP- and TG-treated MTX (A and B), J82 (C and D) and T24 (E and F) cell lines. In contrast to Figure 6, the present factorial plane is defined by the first and the third canonical functions. The rest of the legend is identical to that of Figure 6.

for each cell line. Area I included the folic acid antagonist, i.e. MTX. Area II included the pyrimidine analogs, i.e. 5-FU and ARA-C. Area III included the purine analogs, i.e. MP and TG.

Discussion

Several recent papers focus on the study of the antineoplastic drug-induced effects in cell biology by means of morphonuclear digital cell image analysis.[7,21–24] This methodology makes it possible to monitor drug-induced effects at several levels of tumor cell biology. We demonstrated previously that the computerized analysis of nuclear images submitted to multivartiate analysis enables a parallel study to be undertaken of the cytotoxic effects of antineoplastic agents together with their effects on cell kinetics and chromatin texture. At the same time, it also makes it possible to characterize certain molecules according to their operating mechanisms.[7] In the present work, we use this methodology in order to discriminate between operating mechanisms of antimetabolites agents. This process was carried out in relation to their effect on the chromatin pattern. For this purpose, use was made of MTX, which is an inhibitor of the dihydrofolate reductase; 5-FU and ARA-C, which are two pyrimidine analogs; and MP and TG; which are two purine

Table 4. Linear discriminant analysis performed on each experimental condition studied in comparison with the CT of the corresponding cell line

	Concentration (M)	Cell line		
		MTX	J82	T24
MTX	10^{-8}	93:2092 (CV)		86:1043 (NA)
	10^{-7}		88:1153 (CV)	
5-FU	10^{-7}	83:731 (VOD)		
	10^{-6}		88:1336 (CV)	70:221 (SK)
	10^{-5}		92:1619 :(CV)	63:128 (SK)
	10^{-4}			84:469 (SK)
ARA-C	10^{-7}			82:405 (NA)
	10^{-6}	94:2038 (RLP)	88:2200 (CV)	88:1877 (CV)
MP	10^{-6}	62:49 (VOD)		70:411 (SK)
	10^{-5}	65:143 (SK)		59:23 (LRL)
	10^{-4}	77:496 (SK)	73:358 (SK)	
	10^{-3}		75:226 (SK)	
TG	10^{-8}	67:154 (CV)		67:225 (SK)
	10^{-7}	62:128 (NA)		73:364 (SK)
	10^{-6}	77:458 (SK)	81:1059 (CV)	72:377 (IOD)
	10^{-5}	72:70 (K)		

The '*a*:*b*' values obtained with each experimental condition studied in comparison with the corresponding CT cells. The '*a*' values in percentages represent the level of discrimination and the '*b*' values the discriminatory power of the most discriminatory parameter. According to the Fisher table, an '*a*' value higher than 6 corresponds to a statistical of $p < 0.05$, and '*a*' value higher than 12 corresponds to a statistical level of $p < 0.01$ and an '*a*' value higher than 30 corresponds to a statistical level of $p < 0.001$. This most discriminatory parameter is put in brackets.

analogs. The biological model involved the *in vitro* use of the MTX mouse mammary and the J82 and T24 human bladder cancer cell lines.

The results show that all the antimetabolites tested here caused a significant decrease in the percentage of cells in the G_0–G_1 phase of the cell cycle and a parallel increase in the percentages of cells in the S and/or G_2 phases. No statistically significant effects were observed in the M phase of the cell cycle.

The arrest of cells in the S phase of the cell cycle is a well-known antimetabolite agent-induced effect.[25] The present results also show that these drugs were able to induce the arrest of the cells in the G_2 phase of the cell cycle. This result is also corroborated by previous ones reported in the literature. Indeed, it has been proved that the two purine analogs are able to block cells both in the S and in the G_2 phases of the cell cycle.[6,26] In view of the fact that MTX, 5-FU and ARA-C induce DNA strand breaks,[27–30] it is not surprising that they are also able to bring about a G_2 arrest of the cells in the same way as certain alkylating agents which also induce DNA strand breaks.[31]

The results from the computer-assisted microscope analysis show that the five drugs under study produced similar effects, i.e. an increase in the mean value of the NA, IOD, LRL and LM parameters. This was revealed by the monovariate analyses. These drug-induced increases in the mean NA, IOD, LRL and LM parameter values correspond to the fact that the drug treatment brought about an increase in the nuclear DNA content (as assessed by the IOD parameter) followed by an enlarged nuclear size (assessed by the NA parameter). In consequence, the chromatin became more and more condensed (as assessed by both the LRL and LM parameters).

The results also show that the effects of a given drug recorded at the morphonuclear level often develop as a function of the drugs' concentration. Two exceptions were observed in the case of the IOD parameter: the IOD values produced by TG on the MTX cell line at a concentration of 10^{-5} M were weaker than those recorded at the lower concentrations. The same observation was made when the effects of the 10^{-5} M MP on the T24 cell nuclei were considered. We attribute this decrease in the mean IOD value to the fact that at the highest concentrations, the antimetabolites caused the death of the more sensitive cells. So the remaining cells were the more chemoresistant cells and consequently slightly modified by the treatment. This hypothesis is corroborated by the fact that the highest drug concentrations did not have any significant effects on the cell cycle even though the lower concentration did bring about an

increase in the percentage of cells in the G_2 phase (see Table 3).

Due to the fact that all the antimetabolites under study produced apparently similar effects (e.g. increases in the NA, IOD, LRL or LM values as compared with the CT values) when assessed by monovariate statistical analysis, the results of monovariate analysis alone did not make it possible to discriminate the drugs in terms of their operating mechanisms. This is the reason why we used the multivariate analysis of the drug-induced modifications at the morphonuclear level. This multivariate analysis is related to the use of principal component analysis followed by the canonical transformation of the data. This statistical and mathematical treatment of the data makes it possible to characterize 'typical' cell nuclei from the nuclear populations treated with the different antimetabolites under study. The projection of the multivariate analysis-related results onto the factorial plane given by the first two canonical functions (Figure 6) enabled us to distinguish between the folate antagonist (MTX) and the two purine antagonists (MP and TG). Indeed, the MTX was situated under the positive values of the first canonical function describing the canonical space, while the purine antagonists were situated under the negative values of this canonical function. Unfortunately, it was not possible to assign a specific zone of the plane to the two pyrimidine antagonists. In contrast, the factorial plane defined by the first and third canonical functions (Figure 7) made it possible to discriminate between the five antimetabolites on the basis of their operating mechanisms. Indeed, on charts A, C and E of Figure 7, it was possible to circumscribe part of the plane for each family of antimetabolites: the folate antagonist MTX was always located under the positive values of the first canonical function (area I), as is mentioned above; the two pyrimidine antagonists, i.e. 5-FU and ARA-C, were always located under the positive values of the third canonical function (area II); while the two purine antagonists, i.e. TG and MP, were always located in the negative area of the first canonical function (area III). So, the use of the multivariate analysis of the drug-induced modifications at the morphonuclear level made it possible to describe a certain specificity in their operating mechanisms. We are now pursuing our experiments with other families of drugs, such as alkylating agents, topoisomerase II inhibitors, vinca alkaloids, etc., for the purpose of establishing a 'map' where it is possible to discriminate between the different drug operating mechanisms by means of their position on this 'map'. This model would make it possible to employ a single and easy method to obtain information about the operating mechanism of new drugs.

Conclusion

In conclusion, the present work shows that anticancer antimetabolites produced specific morphonuclear modifications such as an increase in the nuclear DNA content, with a consequent increase in nuclear size. These phenomena were accompanied by an increase in the frequency of the large dense chromatin clumps within the nucleus and consequently in the overall chromatin condensation. The antimetabolites also induced an increase in the DNA content. The drug-induced increase in the nuclear DNA content can be explained by the percentage of cells arrested in the S and/or G_2 phase of the cell cycle.

The present methodology shows that by means of multivariate analysis and by reference to well-known compounds it would be relatively easy to locate an unknown, i.e. an investigational agent, in terms of operating mechanism. Furthermore, the present study also shows that the effects caused by a given drug on tumor cell biology can be monitored at several levels, i.e. cell proliferation, cell kinetics and chromatin pattern characteristics, with these latter being directly related to the operating mechanisms of that drug. The present methodology therefore corresponds to a new pharmacological tool making it possible to monitor the effects caused by antineoplastic agents.

References

1. Ross WE, Zwelling LA, Kohn KW. Relationship between cytotoxicity and DNA strand breakage produced by adriamycin and other intercalating agents. *Int J Radiat Oncol Biol Phys* 1979; **5**: 1221–4.
2. Sunters A, Springer CJ, Bagshawe KD, *et al.* The cytotoxicity, DNA crosslinking and DNA sequence selectivity of the aniline mustards melphalan, chlorambucil and 4-(bis(2-chloroethyl)amino) benzoic acid. *Biochem Pharmacol* 1992; **44**: 59–64.
3. Binet S, Fellous A, Lataste H, *et al. In situ* analysis of the action of Navelbine® on various types of microtubules using immunofluorescence. *Semin Oncol* 1989; **16**: 5–8.
4. Jordan MA, Thrower D, Wilson L. Mechanism of inhibition of cell proliferation by Vinca alkaloids. *Cancer Res* 1991; **51**: 2212–22.
5. Jolivet J, Schilsky RL, Bailey BD, *et al.* Synthesis, retention, and biological activity of methotrexate polyglutamates in cultured human breast cancer cells. *J Clin Invest* 1982; **70**: 351–60.

6. Bökkerink JPM, Stet EH, De Abreu RA, *et al.* 6-Mercaptopurine: cytotoxicity and biochemical pharmacology in human malignant T-lymphoblasts. *Biochem Pharmacol* 1993; **45**: 1455–63.
7. Pauwels O, Kiss R. The application of computerized analysis of nuclear images and multivariate analysis to the understanding of the effects of antineoplastic agents and their mechanism of action. *Methods Find Exp Clin Pharmacol* 1993; **15**: 113–24.
8. Kiss R, Salmon I, Camby I, *et al.* Characterization of factors in routine laboratory protocols that significantly influence the Feulgen reaction. *J Histochem Cytochem* 1993; **41**: 935–45.
9. Kiss R, Devleeschouwer N, Paridaens R, *et al.* Phenotypic change of the transplantable MTX mammary adenocarcinoma into mixed bone producing sarcoma-like tumors. *Anticancer Res* 1986; **6**: 753–60.
10. O'Toole C, Price ZH, Ohnuki Y, *et al.* Ultrastructure, kariology and immunology of a cell line originated from a human transitional-cell carcinoma. *Br J Cancer* 1978; **38**: 64–76.
11. Bubenik J, Baresova M, Jakoubkova J, *et al.* Established cell line of urinary bladder carcinoma (T24) containing tumour-specific antigen. *Int J Cancer* 1973; **11**: 765–73.
12. Black D, Livingstone RB. Antineoplastic drugs in 1990. A review (Part I). *Drugs* 1990; **39**: 489–501.
13. Watson CS, Medina D, Clark JH. Estrogen receptor characterization in a transplantable mouse mammary tumor. *Cancer Res* 1977; **37**: 3344–8.
14. Brugal G, Garbay C, Giroud F, *et al.* A double scanning microphotometer for image analysis: hardware, software and biomedical applications. *J Histochem Cytochem* 1979; **27**: 144–52.
15. Kiss R, Gasperin P, Verhest A, *et al.* Modification of tumor ploidy level via the choice of tissue taken as diploid reference in the digital cell image analysis of Feulgen-stained nuclei. *Modern Pathol* 1992; **5**: 655–60.
16. Galloway MM. Texture analysis using gray run lengths. *Computer Graphics Image Processing* 1975; **4**: 172–9.
17. Haralick RM, Shanmugam T, Dinstein I. Textural features for image classification. *IEE Trans Syst Man Cybern* 1973; **3**: 610–20.
18. Bartels PH. Numerical evaluation of cytologic data. V. Bivariate distributions and the Bayesian decision boundary. *Anal Quant Cytol* 1980; **11**: 433–9.
19. Etievant C, Kruczynski A, Pauwels O, *et al.* The combination of the tetrazolium derivative reduction (MTT) and digital cell image analysis to monitor in vitro the cytotoxicity of anti-neoplastic drugs. *Anticancer Res* 1991; **11**: 305–12.
20. Gozy M, Pauwels O, Gasperin P, *et al. In vitro* characterization of radiotherapy-induced morphonuclear modifications on chemosensitive as opposed to chemoresistant neoplastic cells. *Int J Radiat Oncol Biol Phys* 1993; **27**: 83–91.
21. Kiss R, de Launoit Y, Gras S, *et al.* A new assay to evaluate cell growth and drug sensitivity in culture using a cell image processor. *Anticancer Res* 1988; **8**: 765–74.
22. Colomb E, Dussert C, Martin PM. Nuclear texture parameters as discriminant factors in cell cycle effect and drug sensitivity studies. *Cytometry* 1991; **12**: 15–25.
23. Briffod M, Spyratos F, Hacène K, *et al.* Evaluation of breast carcinoma chemosensitivity by flow cytometric DNA analysis and computer assisted image analysis. *Cytometry* 1992; **13**: 250–8.
24. Pauwels O, Kiss R. Monitoring of chemotherapy-induced morphonuclear modifications by means of digital cell image analysis. *J Cancer Res Clin Oncol* 1993; **19**: 533–40.
25. Hill BT. Cancer chemotherapy. The relevance of certain concepts of cell kinetics. *Biochim Biophys Acta* 1978; **516**: 389–417.
26. Wotring LL, Roti Roti JL. Thioguanine-induced S and G_2 blocks and their significance to the mechanism of cytotoxicity. *Cancer Res* 1980; **40**: 1458–62.
27. Fram RJ, Kufe DW. DNA strand breaks caused by inhibitors of DNA synthesis: 1-β-D-arabinofuranosylcytosine and aphidicolin. *Cancer Res* 1982; **42**: 4050–3.
28. Li JC, Kaminskas E. Accumulation of DNA strand breaks and methotrexate cytotoxicity. *Proc Natl Acad Sci USA* 1984; **81**: 5694–8.
29. Golos B, Malec J. Enhancement of methotrexate-induced growth inhibition, cell killing and DNA lesions in cultured L5178Y cells by the reduction of DNA repair efficiency. *Biochem Pharmacol* 1989; **38**: 1743–8.
30. Willmore E, Durkacz BW. Cytotoxic mechanisms of 5-fluoropyrimidines. Relationships with poly(ADP-ribose) polymerase activity, DNA strand breakage and incorporation into nucleic acids. *Biochem Pharmacol* 1993; **46**: 105–211.
31. Frankfurt OS, Seckinger D, Sugarbaker EV. Flow cytometry analysis of DNA damage and repair in the cells resistant to alkylating agents. *Cancer Res* 1990; **50**: 4453–7.

(Received 28 December 1993; accepted 20 January 1994)